804

UNIVERSITÉ DE NEUCHÂTEL FACULTÉ DES SCIENCES

THÈSE

présentée à la Faculté des Sciences de l'Université de Neuchâtel
pour l'obtention du grade de docteur ès sciences
par

ERIC BOVET
physicien diplômé de l'Université de Neuchâtel

1.B;2.B

Nuclear Physics A304 (1978) 29–39; © *North-Holland Publishing Co., Amsterdam*

NEUTRON-NEUTRON QUASIFREE SCATTERING IN THE ^{2}H(n, nn)p REACTION AT E_n = 14.1 MeV

E. BOVET, F. FOROUGHI and J. ROSSEL

Neuchâtel University, Institute of Physics, CH-2000 Neuchâtel, Switzerland

Received 22 March 1978

Abstract: Neutron-neutron quasifree scattering has been studied in the deuteron break-up reaction ^{2}H(n, nn)p at E_n = 14.1 MeV. Two coplanar and symmetric configurations have been investigated in a kinematically complete experiment where the detection of the spectator particle was not possible. The experimental cross sections are compared with "exact" calculations derived from Faddeev-type equations solved with S- and P-wave nucleon-nucleon separable interactions. These calculations agree both in shape and magnitude with the differential cross section for the $\theta_1 = -\theta_2 = 40°$ configuration ($E_p^{min} = 0$). At $\theta_1 = -\theta_2 = 30°$ (E_p^{min} = 180 keV), however, the absolute value of the measured cross section is too high and an observed structure in the shape of the differential cross section is in sharp conflict with the now available "exact" calculations.

E | NUCLEAR REACTION ^{2}H(n, 2n)p, E = 14.1 MeV, measured $\sigma(E_1, E_2, \theta_1, \theta_2)$.

1. Introduction

In recent years, the three-nucleon system has been extensively studied both experimentally and theoretically. One major reason for this development is that, after the pioneering work of Faddeev [1]), one can calculate exactly the various properties of the three-nucleon bound and scattering states if a two-nucleon interaction model is given as an input.

The purpose of studying the nucleon-deuteron break-up reaction is essentially the following:

(i) A systematic analysis of the most important reaction mechanisms, in particular the well-known final-state interaction (FSI) and quasifree scattering (QFS) processes.

(ii) A quantitative comparison between experiment and "exact" calculations.

(iii) The determination of the nucleon-nucleon low energy scattering parameters.

The nucleon-deuteron system has been studied in many complete experiments using incident protons at energies between 10 and 50 MeV, detecting two particles in coincidence at a variety of angles. Kinematically complete neutron-deuteron experiments have been less frequent, suffering from high background rates and low statistical accuracy. There are over 20 publications which are specifically set up to study p-p or n-p QFS below 50 MeV [ref. [2])]. On the other hand, there is only one

preliminary measurement in the vicinity of n-n QFS at 14.1 MeV [ref. [3])]. Therefore, our measurement will be filling an important gap in this domain.

A kinematically complete measurement of the ^{2}H(n, nn)p reaction with the detection of the two outgoing neutrons is very long and difficult to perform, but has the advantage of excluding Coulomb interaction. Therefore, low energy experimental cross sections can be compared directly with theoretical predictions based on Faddeev equations. These theoretical predictions do not take the Coulomb interaction rigorously into account and most of them are restricted to S-wave nucleon-nucleon interactions.

Our purpose in this paper is to show that a neutron-neutron quasifree scattering experiment is technically feasible. The results are compared with several recent models based on "exact" solutions of Faddeev equations. We have measured the fivefold differential cross section for the ^{2}H(n, nn)p reaction at two different symmetric kinematical configurations enhancing neutron-neutron quasi-free scattering. The first configuration, $\theta_1 = -\theta_2 = 40°$, corresponds to a zero minimum energy of the spectator proton (exact QFS point) and the second one, $\theta_1 = -\theta_2 = 40°$ ($E_p = 180$ keV), corresponds to the configuration chosen by Šlaus *et al.* [3]) in their preliminary measurement.

In sect. 2, we describe the kinematics of the experiment and the calculations based on Faddeev-like equations. Sect. 3 is devoted to the description of the experimental procedure and data analysis. Finally, conclusions are drawn in sect. 4.

2. Theory

2.1. KINEMATICS

The three momenta of the final state bodies in the reaction a + b → 1 + 2 + 3 are constrained by the kinematic equations of conservation of energy and momentum. If each body is parametrized by three variables, namely two angles and the kinetic energy, and provided the initial state is completely known, the number of degrees of freedom in the final state is reduced to five. In the present experiment, these variables are determined as follows. Two particles are detected in two fixed directions characterized by two polar and azimuthal angles ($\theta_1, \phi_1, \theta_2, \phi_2$) and the energy of each one (E_1 and E_2) is determined. The knowledge of six parameters with the simultaneous detection of E_1 and E_2 constitutes a useful basis for eliminating background events.

2.2. DYNAMICS

The fivefold differential cross section for a three-particle reaction, in the case of a target particle b at rest, can be written in the lab system in the following way [4]):

$$\frac{d^5\sigma}{d\Omega_1 d\Omega_2 dE_1} = \frac{2\pi m_a}{k_a}|U_{0a}|^2\rho(E_1),$$

where $\rho(E_1)$ is the phase-space factor given by

$$\rho(E_1) = \frac{m_1 m_3 k_1 k_2^2}{\hbar^4((m_2+m_3)/m_2)\, k_2 + k_1 \cos\theta_{12} - k_a \cos\theta_2)}.$$

The quantities m_i and $\hbar k_i$ are the mass and momentum of particle i, and θ_{12} is the angle between $\boldsymbol{k}_1$ and $\boldsymbol{k}_2$. The matrix element U_{0a} is the on-shell solution of the so-called AGS equations [5]):

$$U_{\beta\alpha} = (1-\delta_{\beta\alpha})G_0^{-1} + \sum_\gamma U_{\beta\gamma} G_0 t_\gamma (1-\delta_{\gamma\alpha}) \qquad (\alpha, \beta = 0, 1, 2, 3),$$

where $G_0(E) = (E-H_0)^{-1}$ is the free three-particle Green function and t_γ is the two-body off-shell nucleon-nucleon transition matrix in the three-particle space.

These AGS equations constitute the starting point of most of the existing "exact" calculations. These "exact" calculations contain no free parameters and require as input only the knowledge of the on-shell and off-shell two-body transition amplitudes t_γ. In the realistic case of three interacting nucleons, and after partial-wave decomposition, these equations constitute a set of coupled integral equations in two continuous variables. Therefore simplifying hypotheses on the nucleon-nucleon interaction must be made in order to solve these equations numerically.

The separable approximation is the most widely used approximation in three-nucleon calculations because (i) it reduces the AGS equations to a set of one-variable integral equations and (ii) this approximation reflects the fact that the nucleon-nucleon interaction at low energies is dominated by the presence of the bound and unbound state poles of the deuteron. The generally used separable interactions, differing in the parametrization of their form factors, do fit the nucleon-nucleon low energy effective range parameters (see table 1).

Three different calculations have been used in this work:

(i) The calculations of Ebenhöh [6]), which are restricted to S-wave nucleon-nucleon interaetions. These calculations are performed using a hybrid treatment of the nucleon-nucleon charge dependence.

(ii) Exact charge dependent calculations obtained from a modified Ebenhöh code [7]).

TABLE 1

Nucleon-nucleon scattering parameters (in fm)

	Ebenhöh	Bruinsma
a_{nn}	−16.0	−20.3
a^s_{np}	−23.7	−20.3
a^t_{np}	+ 5.4	+ 5.4
r_{nn}	2.86	2.7
r^s_{np}	2.67	2.7
r^t_{np}	1.75	1.7

(iii) The calculations of Bruinsma [8]), including P-wave interactions and the tensor force. These are, however, charge independent calculations (see table 1).

3. Experiment

3.1. DESCRIPTION OF THE APPARATUS

The experimental set-up is shown in fig. 1. The 14.1 MeV neutrons, produced by the ^{3}H(d, n)^{4}He reaction, were incident on a spherical C_6D_{12} target (diameter 4 cm). The neutron beam was collimated both geometrically by a beam-pipe through a Fe-Pb-paraffin shielding and electronically by the associated α-particle method [9]).

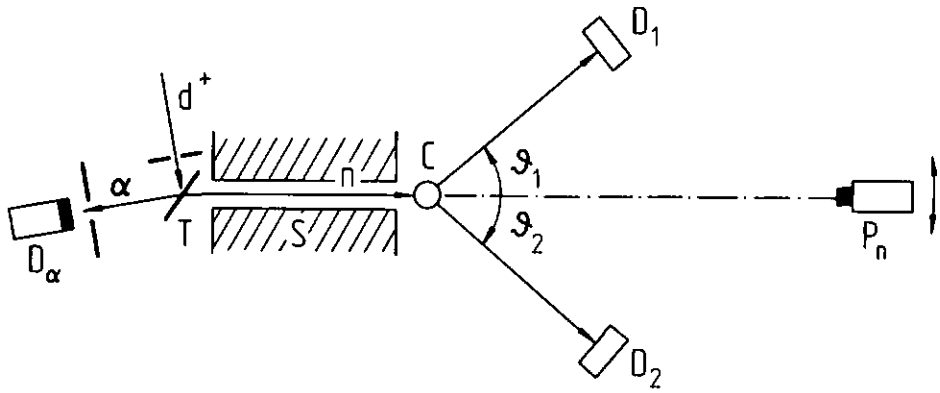

Fig. 1. Experimental set-up. T: rotating tritium target (TiT); S: shielding (iron-lead-paraffin); C: C_6D_{12} liquid target; D_α: α-particle detector; D_1 and D_2: neutron detectors; P_n: neutron beam profile monitor. Distances: T-C = 100 cm; C-D_1 = C-D_2 = 120 cm. Acceptance solid angles of detectors $\Omega_1 = \Omega_2 =$ 15 msr.

The outgoing break-up neutrons were detected by two NE 213 liquid scintillators D_1 and D_2 ($15 \times 15 \times 4$ cm^3), placed 120 cm from the target and at symmetric angles $\theta_1 = -\theta_2$ about the beam axis. For each break-up event, a reference point in time was obtained by detecting the α-particle associated with the neutron emission at the source. The time differences, $TOF_{\alpha-N1}$ and $TOF_{\alpha-N2}$, between the detection of the α-particle and the break-up neutrons were measured simultaneously.

In a typical complete experiment, the detection of the break-up proton in a scintillating target is usually used to reduce background effectively. But this was not possible in this experiment, because kinematically the proton energy was minimum (almost zero) at the point of QFS. Therefore, particular attention was paid to reduce the background by other means. These were the following:

(i) A pulse-shape discrimination system (PSD) [10]) was applied to the outputs of both neutron detectors.

(ii) An optimum energy threshold was imposed on each detector in the off-line treatment in order to eliminate the low energy background neutrons.

(iii) A semi-automatic device P_n, consisting of a small plastic scintillator, was used to monitor the neutron beam profile in order to check the angular stability of the incident neutron beam during the experiment.

The absolute value of the break-up differential cross section was determined by comparison with elastic ^{2}H(n, n)^{2}H and ^{12}C(n, n)^{12}C cross sections. This has the considerable advantage that elastically scattered neutrons were detected in the present experiment, interspersed with the detection of deuteron break-up events. The two processes sample the same incident neutron beam and, furthermore, are sensitive to the same effective target volume.

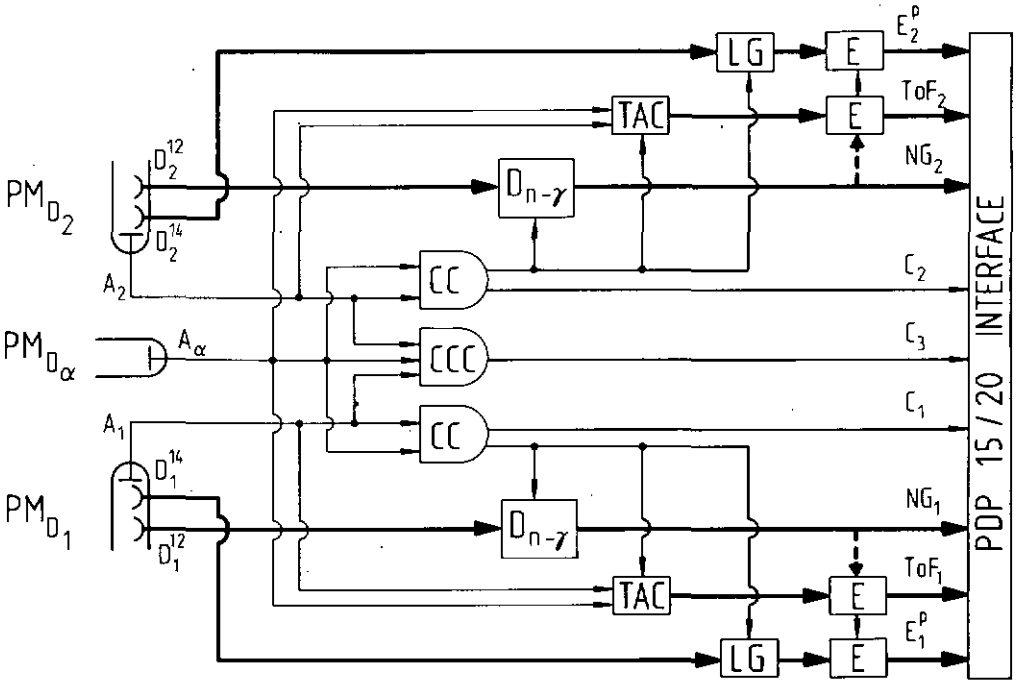

Fig. 2. Block diagram of the electronic circuitry. PM: photomultiplier; A_i, D_i^{14}, D_i^{12}: anode and dynode outputs; CC, CCC: double and triple coincidence modules, respectively; $D_{n-\gamma}$: pulse-shape discrimination circuit; TAC: time-to-amplitude converter; LG: linear gate and stretcher module; E: encoders.

The signals from the three detectors D_α, D_1 and D_2 were firstly processed by the electronic set-up which is shown in fig. 2. Each of the two neutron detectors consisted of a NE 213 liquid scintillator optically coupled to the photocathode of a type 56 DVP photomultiplier and had three outputs: (i) an anode pulse $A_{1,2}$ used for fast timing information, (ii) a dynode pulse $D_{1,2}^{14}$ derived from the 14th dynode, which was used for the determination of the proton recoil energy $E_{1,2}^p$ in the scintillators and (iii) a dynode pulse $D_{1,2}^{12}$ derived from the 12th dynode and entering into a n-γ pulse-shape discrimination circuit which has been described in ref. [10]).

The block diagram of the electronics (see fig. 2) contained three sections:

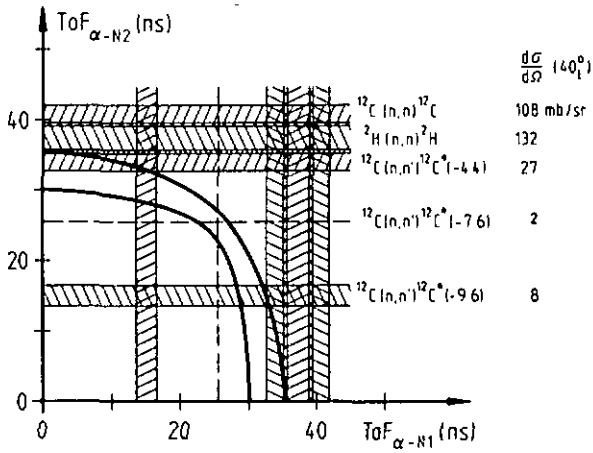

Fig. 3. Contamination of the break-up neutrons kinematical locus in the $TOF_{\alpha-N1} - TOF_{\alpha-N2}$ matrix from the $^{12}C(n, n')^{12}C^*$ reactions, for the $\theta_1 = -\theta_2 = 40°$ configuration. The thick lines delimit the extreme kinematical loci compatible with the finite aperture of the detectors. The width of the horizontal and vertical bands is due to the instrumental time-of-flight resolution.

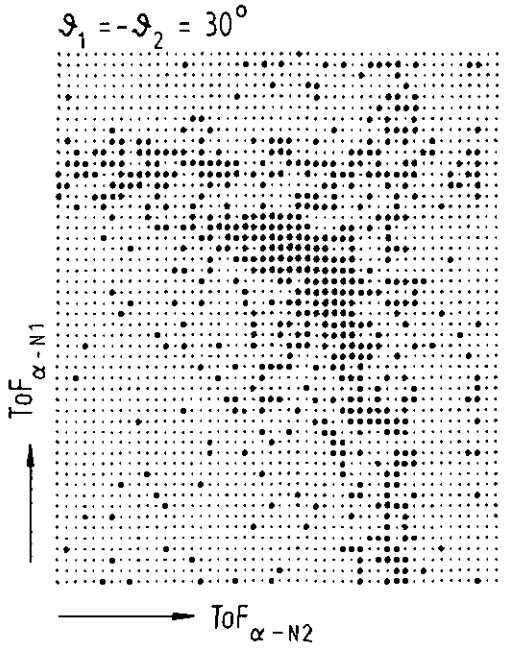

Fig. 4. Two-parameter spectrum of n-n coincidences from the break-up reaction $^2H(n, nn)p$, for the $\theta_1 = -\theta_2 = 30°$ configuration.

(a) *The timing information* (thin lines in fig. 2): this section consisted of the pulses $A_{1,2}$ and A_α, which activated the time-to-amplitude converter module (TAC) after passing through a triple (CCC) or double (CC) coincidence module (used to discriminate between break-up and elastic events).

(b) *The spectroscopic information* (broad lines in fig. 2): this section was formed

by the $D^{14}_{1,2}$ pulses feeding the linear gate and stretcher module (LG). The four signals (TOF_1, E^p_1, TOF_2, E^p_2) defining a break-up event were then digitalized by four 20 MHz encoders (E) and were read by a PDP 15/20 computer through an appropriate CAMAC interface.

(c) *The logic*: this section is made up of three subsections, namely (i) the n-γ PSD system, (ii) the system for the identification of break-up and elastic events, (iii) a scaler system (the different count rates were picked up at six different points of the circuit and were used to test the stability of the overall system during the data acquisition).

The break-up and elastic events were recorded on a magnetic tape for a detailed off-line treatment. The accumulation of these events were constantly controlled by an on-line display unit. As an example, fig. 4 shows the events populating the kinematical locus in the $TOF_{\alpha-N1}$-$TOF_{\alpha-N2}$ matrix (50×50 channels) taken from 500 h of accumulation at $\theta_1 = -\theta_2 = 30°$.

The contamination of the QFS kinematical locus for the two break-up neutrons from the inelastic ^{12}C(n, n')^{12}C* reactions is clearly shown in fig. 3. The detection of inelastically scattered neutrons in one detector, in coincidence with accidental events in the other, might cause the appearance of a band structure which, in the case of the ^{12}C(n, n')^{12}C*($Q = -7.6$ MeV) reaction, could be fatal in such a measurement. However, at angles $30° \lesssim \theta \lesssim 50°$, the differential cross section for this reaction is extremely low [11]). Moreover, the magnitude of this contamination can be estimated by comparison with the yield of the ^{12}C(n, n')^{12}C*($Q = -9.6$ MeV) reaction. This can easily be evaluated, being 3–5 times larger and because its contribution lies outside the break-up kinematical curve. In fact, fig. 4 shows that, apart from the two bands due to the elastic ^{2}H(n, n)^{2}H and ^{12}C(n, n)^{12}C reactions, no other bands are visible in the $TOF_{\alpha-N1}$-$TOF_{\alpha-N2}$ matrix.

With a rate of break-up events of the order of 1 count/h, we have performed two measurements of about 800 h at $\theta_1 = -\theta_2 = 30°$ and 1400 h at $\theta_1 = -\theta_2 = 40°$. These two configurations were alternated in time to ensure the same experimental conditions for the two configurations.

3.2. DATA ANALYSIS – COMPARISON WITH THEORETICAL PREDICTIONS

The analysis has been divided into six important steps:

(i) Analysis of the stability of the data acquisition by sequential inspection of the six control rates. We have been able to constitute three classes of break-up events corresponding to three different degrees of stability of the apparatus.

(ii) Choice of an optimum off-line threshold for the two neutron detectors by inspection of the corresponding signal-to-noise ratio. This threshold has been set at 2 MeV proton by applying a computer cut-off.

(iii) A careful analysis of the neutron and γ background contributions has been undertaken to check the unexpected structure in our $\pm 30°$ results. Additional measurements have been performed with an equivalent carbon target to test the

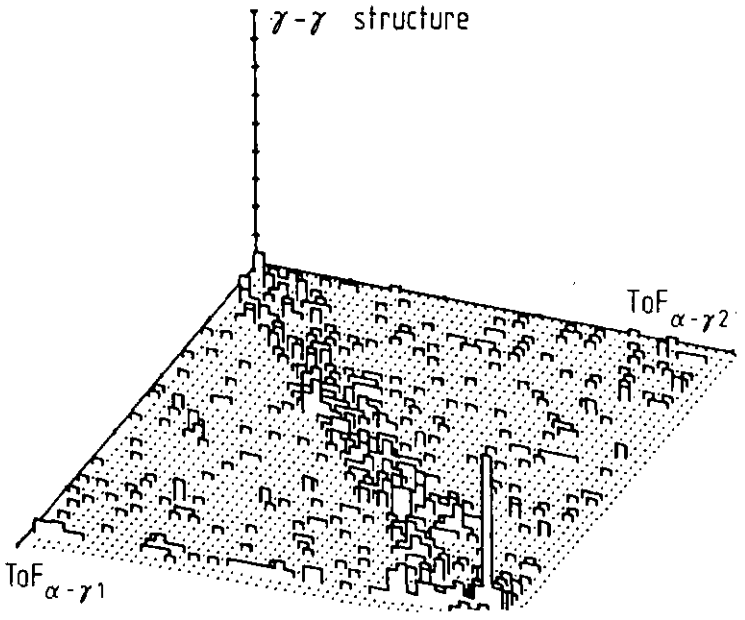

Fig. 5. Two-parameter spectrum of γ-γ coincidences, corresponding to γ-rays Compton scattering from one detector into the other. This spectrum was obtained with a carbon target at $\theta_1 = -\theta_2 = 30°$, and with a γ PSD selection for each detector.

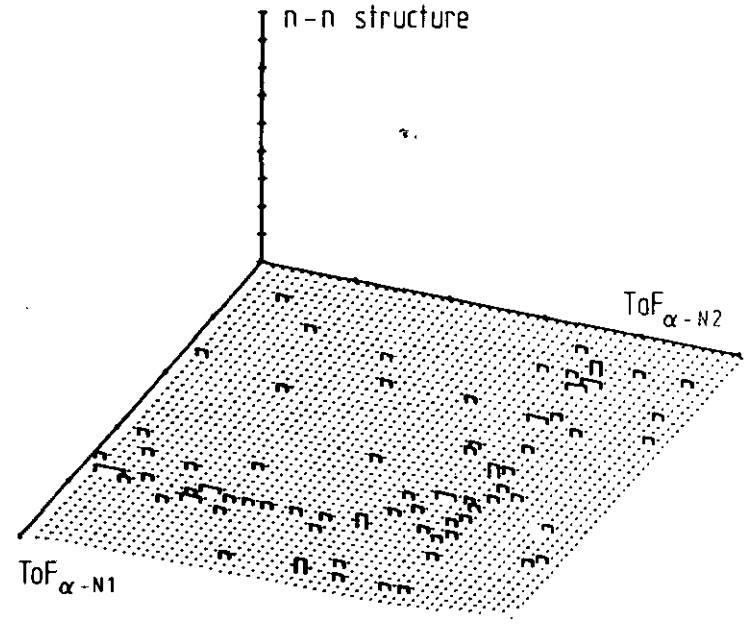

Fig. 6. Neutron-neutron coincidence spectrum corresponding to the same situation as described in fig. 5, but with a neutron PSD selection for each detector.

background contributions resulting from the ^{12}C nuclei. Fig. 5 shows the result of the test with the carbon target, when γ-selection was applied to both detectors. The presence of the events lying inside the double diagonal region is due to γ-rays Compton scattered from one detector into the other. We have observed no effect of this nature when the neutron selection was applied for each detector (see fig. 6).

(iv) An experiment was performed to measure the neutron detection efficiency of the scintillators used in the present experiment. The method of this efficiency measurement was similar to the one described by Lunke *et al.* [9]). These measured efficiencies were used in the calculations of the absolute cross sections.

(v) The absolute break-up cross sections have been determined by summing all elastically scattered neutrons on ^{2}H and ^{12}C nuclei and normalizing to the values which have been taken from refs. [12,13]).

(vi) Finally, neutron multiple scattering events taking place in the C_6D_{12} target have been introduced under the form of a global attenuation factor for the outgoing neutrons.

The background subtracted experimental spectra were projected along both the $TOF_{\alpha-N1}$ and $TOF_{\alpha-N2}$ axes. Because of the choice of symmetric configurations, these two spectra should be the same and in fact they are statistically compatible. Furthermore, the structure appearing in the shape of the $\theta_1 = -\theta_2 = 30°$ differential

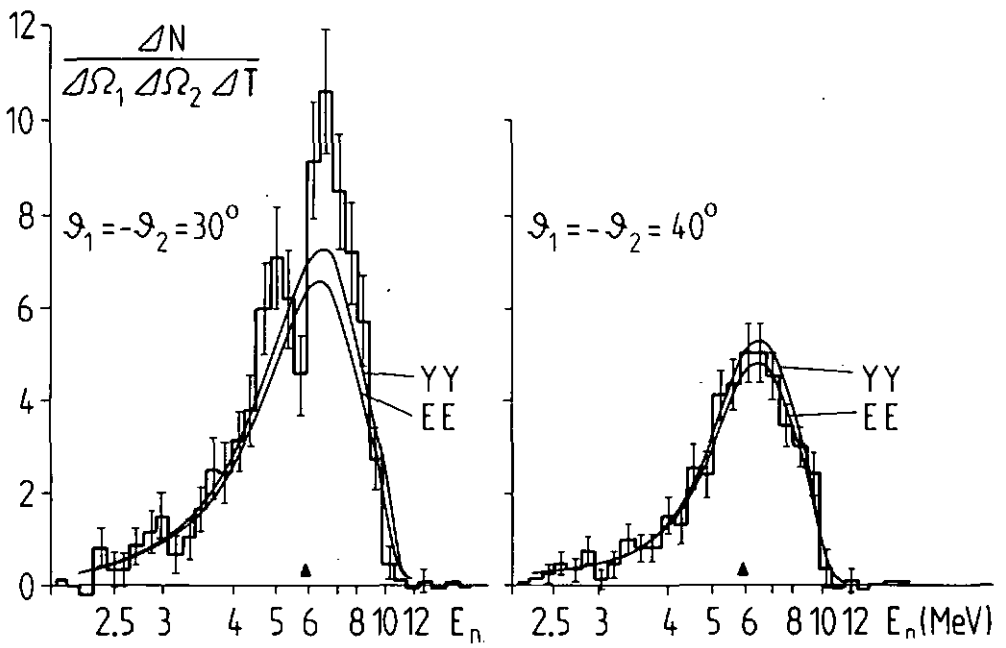

Fig. 7. Comparison of the experimental projections (histograms) and theoretical predictions (solid lines), for the two kinematical configurations. The spectra are projected along their natural TOF axes. The vertical units are normalized to the usual break-up cross section $d\sigma/d\Omega_1 d\Omega_2 dE_n$ (in mb/sr^2 · MeV) at the QFS point indicated by a triangle (▲).

cross section (see fig. 7) has been shown to be independant of any criterion in the off-line treatment, such as the choice of the detector threshold, stability conditions or accidental shift in the n-γ discrimination system.

In fig. 7, we compare our results with the "exact" calculations of Ebenhöh [6]) based on separable rank-one S-wave nucleon-nucleon interactions with a hybrid treatment for the nucleon-nucleon charge dependance. The two curves labelled YY (Yamaguchi-Yamaguchi) and EE (exponential-exponential) correspond to two nucleon-nucleon form factors in the $^1S_0$ and $^3S_1$ states which give the most extreme results. These theoretical curves take into account the finite aperture due to the detectors and the instrumental time-of-flight resolution.

The errors quoted for each datum point include estimates of errors due to counting statistics. The errors in the n-^{2}H and n-^{12}C elastic cross sections to which normalization was made (10 %), the error in the neutron detection efficiency (5 %) and the error due to multiple scattering (5 %) have not been included in order to facilitate updating the data as new measurements become available.

The predictions of exact charge dependant calculations [7]) differs no more than 1 % from the hybrid calculations of Ebenhöh. On the other hand, the results of the charge independent calculations of Bruinsma [8]), including S- and P-wave interactions and tensor force, have not been reproduced in fig. 7 because they give results lying between the two curves YY and EE of Ebenhöh.

4. Conclusions

From an experimental point of view, this work has proved the feasibility of a neutron induced deuteron break-up experiment without detection of the spectator particle. We have been able to study, for the first time, the neutron-neutron quasifree region where the energy of the spectator proton was zero. This kind of experiment was only possible with a performant n-γ discrimination system and a relatively high energy threshold on each detector. This last condition, unfortunately, tends to lengthen the measurements which are already long in this type of experiment (more than 2000 h for our two configurations).

In the case of exact quasifree configuration $\theta_1 = -\theta_2 = 40°$ ($E_p^{min} = 0$), our results are in very good agreement, both in shape and magnitude, with the "exact" calculations of Ebenhöh and Bruinsma. This demonstrates the fact, already verified in the case of the symmetric ^{2}H(p, pp)n reaction, that the present "exact" three-body calculations are able to predict the correct three-body cross sections even with a very simplified nucleon-nucleon interaction. Although the nucleon-nucleon charge dependance treatment is not the same, it can be said that the very close agreement between Ebenhöh's and Bruinsma's calculations reflects the minor importance of P-wave nucleon-nucleon interaction for the differential cross section at these low energies.

The disagreement between experiment and theory for the $\theta_1 = -\theta_2 = 30°$

configuration (E_p^{min} = 180 keV), particularly the appearance of a structure in the shape of the differential cross section, is puzzling. At the present, it is difficult to propose some definite explanation for this structure, and, unfortunately, none of the existing theoretical calculations can simulate this structure. It is yet interesting to remark that this configuration at E_n = 14.1 MeV, as well as another configuration studied by the Uppsala group [14]) at E_p = 10 MeV showing a similar effect, do both correspond to almost symmetric configurations of the three nucleons in their c.m. system. Although some authors have proved that three-body forces and off-shell effects are indistinguishable (see ref. [15])), it would be highly interesting to study further such symmetric configurations, as well as a collinear one similar to that studied by Lambert *et al.* [16]), to see if enhancing or hiding effects of hypothetical three-body forces take place.

The authors are indebted to Dr. W. Ebenhöh and Dr. J. Bruinsma for their kind amiability in making available their results and computer codes. They wish to thank Dr. C. Nussbaum for his help in writing the acquisition program. This work was partially supported by the Swiss National Science Foundation.

References

1) L. D. Faddeev, JETP (Sov. Phys.) **12** (1961) 1014
2) E. Bovet, Thesis, Neuchâtel University (1977)
3) I. Šlaus, J. W. Sunier, G. Thompson, J. C. Young, J. W. Verba, D. J. Margaziotis, P. Doherty and R. T. Cahill, Phys. Rev. Lett. **26** (1971) 789
4) G. G. Ohlsen, Nucl. Instr. **37** (1965) 240
5) E. O. Alt, P. Grassberger and W. Sandhas, Nucl. Phys. **B2** (1967) 167
6) W. Ebenhöh, Nucl. Phys. **A191** (1972) 97
7) J. Bruinsma, private communication (1976)
8) J. Bruinsma and R. van Wageningen, Nucl. Phys. **A282** (1977) 1
9) C. Lunke, J. P. Egger and J. Rossel, Nucl. Phys. **A158** (1970) 278
10) E. Bovet, P. Boschung and J. Rossel, Nucl. Instr. **101** (1972) 315
11) a. P. Kuijper, J. C. Veefkind and C. C. Jonker, Nucl. Phys. **A181** (1972) 545;
b. G. A. Grin, B. Vaucher, J. C. Alder and C. Joseph, Helv. Phys. Acta **42** (1969) 990;
c. R. Bouchez, J. Duclos and P. Perrin, Nucl. Phys. **43** (1963) 628
12) M. Brüllmann, H. Jung, D. Meier and P. Marmier, Helv. Phys. Acta **41** (1968) 435
13) G. A. Grin, B. Vaucher, J. C. Alder and C. Joseph, Helv. Phys. Acta **42** (1969) 990
14) B. Sundqvist, A. Johansson, L. Amten, L. Gönczi, I. Koersner and P. Palmgren, TLU 4/72 Uppsala (1972)
15) D. D. Brayshaw, Phys. Rev. Lett. **32** (1974) 382
16) J. M. Lambert, P. A. Treado, R. G. Allas, L. A. Beach, R. O. Bondelid and E. M. Diener, Few body problems in nuclear and particle physics, Laval University (1974) 531